

Article

Solid State Recycling of Aluminum Alloy Chips via Pulsed Electric Current Sintering

Clemens Nikolaus Cislo ^{1,*}, Bernhard Kronthaler ¹, Bruno Buchmayr ¹  and Christian Weiß ²

¹ Chair of Metal Forming, University of Leoben, 8700 Leoben, Austria;

bernhard.kronthaler@stud.unileoben.ac.at (B.K.); bruno.buchmayr@unileoben.ac.at (B.B.)

² Chair for Process Technology and Industrial Environmental Protection, University of Leoben, 8700 Leoben, Austria; christian.weiss@unileoben.ac.at

* Correspondence: clemens.cislo@unileoben.ac.at

Received: 6 February 2020; Accepted: 6 March 2020; Published: 10 March 2020



Abstract: Based on high energy demand of the primary production and losses during secondary production, alternative recycling of aluminum becomes a popular research topic. Compared to both primary and secondary production of aluminum, solid state recycling offers energy savings and reduced material losses during processing by surpassing an inefficient melting step. In this work, a direct recycling route for machining chips via pulsed electric current sintering (PECS) is evaluated. Therefore, necessary processing steps for a complete recycling route are briefly outlined. After cleansing, EN AW 6082 chips, provided by Neuman Aluminium GmbH, Marktl, Austria, are compacted with variable loads and consolidated via PECS on two separate systems to enable a comparison. Produced specimens are examined with density measurements, optical microscopy and the bonding quality is evaluated by Vickers micro-hardness measurements. In combination with elevated temperature and deformation, applied current promotes consolidation amongst chips and improvements in density, hardness and microstructure are achieved. The results of this work clearly show a positive effect of PECS on the bonding amongst chips, but further research will be necessary to separate and understand influences of single processing parameters. Additionally, all processing steps from collection to consolidation have to be taken into account to achieve industrial implementation.

Keywords: aluminum; recycling; chips; consolidation; sintering

1. Introduction

The demand for aluminum is constantly growing in several industrial sectors, such as aviation and automotive. To reduce energy consumption and related costs of its primary production, recycling of aluminum and its alloys gains popularity. Although metals are predestined and well-suited for systematic recycling through their properties and quantities, re-melting of aluminum always results in losses of material or quality. Through its high electro-negativity, only the even more reactive metals are removable by selective oxidation, which often results in “down-cycling” through impurities, if not sorted and stored properly [1–5]. In different methods of recycling, the sorting and separation applied to the different alloys and the role of contaminants are very important. For the production of aluminum parts, post-processing operations, e.g., machining, produces a large amount of chips out of the same base alloy, therefore, in-situ sorting can be achieved relatively easily at this point. The recycling of chip-based aluminum could play an important role for an economical use of secondary aluminum. Compared to bulk material, aluminum chips exhibit a larger surface to volume ratio, causing a high proportion of passivating surface oxide layers on the to be recycled material. In combination with low bulk densities of chips, it causes an increased amount of melting losses during re-melting. In comparison to the conventional recycling routes based on re-melting, solid state recycling offers

promising options to a further reduction of energy demand and environmental impact through the aluminum industry, by surpassing this melting step [6–8]. In regard to the mechanisms responsible for consolidation, processes can be separated into metal forming, using deformation under high pressure to enable metallic bonding between the particles and powder metallurgy, utilizing time under elevated temperature and in some cases additional pressure to join the separate particles as used in sintering processes. Figure 1 shows the necessary processing steps during solid state recycling to achieve chip-based specimens for both approaches. Through direct processing of chips without an additional milling step to produce powder or granulate, energy efficiency of the powder metallurgical solid state recycling route may be further improved, with a drawback in sintering quality to be evaluated. In order to achieve metallic bonding between individual chips, metallic contact needs to be enabled by partly rupturing the surface oxides and disperse them within the microstructure. Most commonly, metal forming approach is used to achieve desired bonding through severe plastic deformation. As an alternative to enable metallic bonding, pulsed electric current sintering (PECS), a derivate from regular sintering, recently gained interest and therefore is investigated within this research work [9,10].

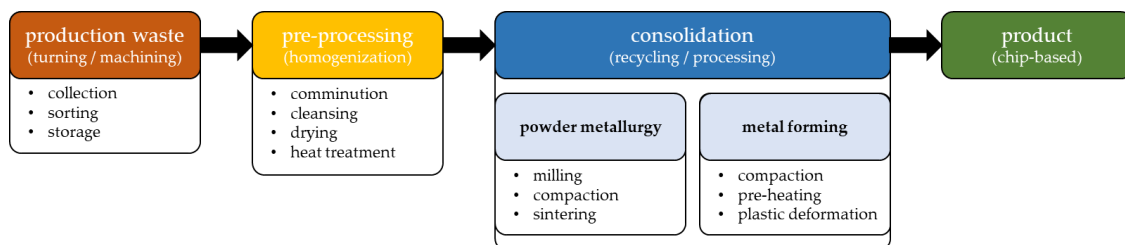


Figure 1. Conventional processing steps during solid state recycling for powder metallurgical and metal forming approaches used to reduce the energy demands during the recycling of aluminum alloy by surpassing a re-melting step.

Pulsed Electric Current Sintering (PECS)

In general, PECS is used to consolidate powder particles, therefore an elimination of gaps and the formation of metallic bonding needs to be achieved to result in desired mechanical properties. To enable dense and well-bonded specimens, mass transport amongst particles needs to be activated. Bonding during PECS is accompanied by a lowering of free energy and with similarities to pressure assisted sintering processes like Hot Pressing (HP), the driving force can be mainly attributed to volume activation through application of external pressure and surface reduction. In the presence of defects, free energy helps to promote the thermally activated matter transport by lattice-, grain boundary- and surface diffusion. A main difference towards HP can be found in the heating mode. As the specimen is heated by applied current through Joule heating, faster heating rates and shorter processing cycles accompanied by lowered sintering temperatures, leading to enhanced material properties and offer economic benefits. Depending on the conductive properties of the powders consolidated this leads to a direct heating through the current for conductive powders, whereas insulating powders will be heated through the conductive dies [11–16]. Figure 2 shows a typical PECS setup, consisting of two punches transferring pressure and current to the container and the specimen. In general, tool materials used for setups like these are good conductors like graphite, but a differing container conductivity can be used to force the current flow towards either container or specimen, depending on the conductivity of the powder material [14]. Depending on the hardware used, electric current is commonly applied in pulses with a duration of a few milliseconds and controlled through temperature measurements [17–19]. According to Zhaohui et al. [20], the pulsed current during sintering results in a spark discharge between particles resulting in the local breakdown of present surface oxides, like in the case of aluminum and its alloys. The discharge further causes a localized melting of the particle surface, resulting in an enhanced neck formation. The process can be divided in the following four subsequent stages:

1. Activation and refining of the powder
2. Formation of sintering necks
3. Growth of sintering necks
4. Densification through plastic deformation

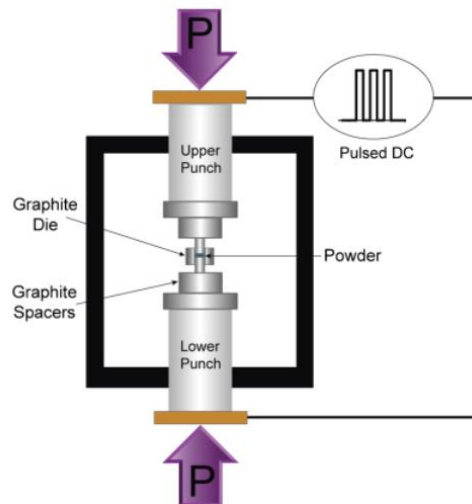


Figure 2. Typical tool setup for pulsed electric current sintering (PECS) with a sample being compressed by graphite punches within a container during simultaneous current application in a vacuum chamber [11].

During the first two stages, the described discharge is likely to occur. Once the necks have been formed, the electric currents flows through the necks and the material is heated by Joule effect and therefore facilitates the densification of the specimen by thermal softening [20,21]. According to Dong et al. [15], the consolidation process starts with micro-arc welding being dominant at the early stages of the process, followed by a stage of electric resistance welding, where joining of the particles is promoted by Joule heating. At the final stage of the process, diffusion welding takes place. Through the electrical field applied, accelerated mass transport is possible and results in a strong metallurgical bond, but its positive effect cannot be clearly separated from temperature effects. Occurrence of spark discharge and the resulting presence of plasma facilitating neck formation is associated with a surface cleansing effect, but on the other hand sparks may also cause localized overheating and melting. In combination with density gradients within pre-compacts, these thermal hotspots cause uneven temperature distribution during processing and therefore may cause inhomogeneity within sintered specimens. As there are some discrepancies concerning the mechanisms responsible for the consolidation, several other terms like spark plasma sintering (SPS) and electric current assisted sintering (ECAS) are describing similar processes utilizing pressure and current to achieve the desired bonding between metallic particles. Some of the bonding mechanisms discussed, like the occurrence of a spark discharge or plasma, are very controversial and others, like diffusion welding, are widely accepted amongst the researchers [11,12,15,22,23]. Although PECS and the other similar processes most commonly are used for powder materials, there already is research available on the successful processing of aluminum chips by Paraskevas et al. [24,25] referring to the same effects during consolidation as stated above. By mixing chips from scrap with atomized powders, they were able to produce samples with no porosity exceeding 35 μm . In comparison to samples produced from powder only, the chip-based specimens could result in an anisotropic material behavior due to a possible alignment of the irregular chips during processing [24]. To reduce this anisotropic behavior, it seems to be reasonable to reduce and homogenize the size of the chips by milling, but according to Wan et al. [10] the rising ratio between surface oxide and volume needs to be taken into account as a main influence on the consolidation

behavior. Through the increasing surface to volume ratio, the amount of oxides in the specimens increases accordingly, further suppressing the metallic bonding between the particles.

As only limited amount of research and processing parameters are available for solid state recycling of chips using PECS, this research aims to further evaluate the feasibility of these powder metallurgical approaches, collectively called pulsed electric current sintering. Therefore, chip-based EN AW-6082 specimens are produced via PECS at the University of Leoben, utilizing a Gleeble 3800 thermo-mechanical treatment simulator, manufactured by DSI, El Segundo, CA, USA. As this system uses pulse-width-modulated (PWM) AC for sample heating, additional experiments with a specific spark plasma sintering machine using pulsed DC at the technical University Bergakademie Freiberg (TU BA Freiberg), in the following denoted as SPS, are conducted for comparison. Results are assessed via density evaluation, optical microscopy and Vickers hardness measurements. Additionally, a short overview about necessary processing steps and preparatory work prior to consolidation is given, to briefly discuss topics regarding solid state recycling often neglected in literature.

2. Materials and Methods

Aluminum chips used during the experiments performed in this work were produced for the purpose to verify different solid-state recycling routes only and, therefore, they are more homogenous than regular chips and machining swarf from production. Although all chips were based on EN AW 6082 specimens in T6 tempering state, their structures may differ depending on the amount of temperature arising from machining. These variations can be seen by varying amounts of the darker intermetallic magnesium silicide (Mg_2Si) phase illustrated in Figure 3. Some of the adjoining chips are in a soft annealed tempering state and an unequal composition has to be expected amongst all chips. The brighter and more evenly distributed intermetallic phase mainly consists of the alloying elements iron, manganese and silicon and builds an undissolved and more evenly distributed always present phase of $Al(FeMn)Si$ as published in [26,27]. The mainly spiral machining chips were produced on a conventional lathe with varying processing speeds and amounts of lubrication. This results in thickness variation ranging from approximately one to five millimeters and a highly variable length with some chips exceeding 200 mm. Prior to any further examinations, a comminution step in a double shaft shredder was executed to get a more homogenous blend of chips, averaging in a length of 30 mm and therefore facilitate handling, eliminate possible size-effects regarding sintering and further enhance the comparability amongst individual specimens.

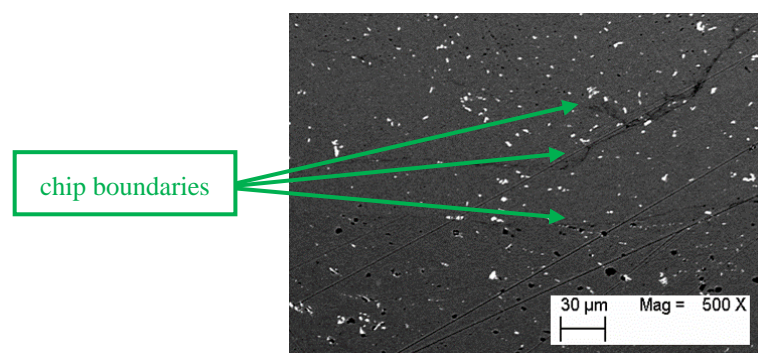


Figure 3. Scanning electron microscope (SEM) picture at 500x magnification of a chip-based briquette prior to pyrolysis, with an uneven distribution of the intermetallic Mg_2Si -phase amongst adjoining chips [26].

2.1. Cleansing

Even though high storage times may reduce residual contents of cooling lubricants to approximately 2–4 weight% and briquetting of the chips would lead to further degreasing of the specimens, an additional cleansing step is necessary to remove residue traces of lubricants and facilitate

the bonding between single particles. All chips have been degreased with acetone in an apparatus similar to a washing drum and dried in a convection oven as presented in previous work [6]. To evaluate the cleansing results, all chips underwent pyrolysis of five to ten hours under atmospheric conditions at 400 °C. Due to the pyrolysis, the structure of the individual chips used during the experiments is almost homogeneous after cleansing, as it equals a soft annealing heat treatment. Therefore, this needs to be taken into account when processing chips with different structures, as the cycle times during PECS may be too short to ensure a homogeneous structure after processing. Nevertheless, a subsequent quenching processes immediately after PECS is not possible with most common tooling assemblies and will result in the necessity of a separate heat treatment for age-hardening aluminum alloys anyway. Additionally, growth of the surface oxides has to be expected due to temperature exposition under atmospheric conditions, even though temperatures were chosen to result in as little oxidation as possible [28,29]. Nevertheless, a possible variation in thickness of the oxides among different chips has to be expected, but detailed examination will not be part of the presented research. A contamination through foreign metals and alloys is considered unlikely and insignificant for the small amounts of chips specifically produced for the scope of this research. Therefore, a cleansing step to remove possible metallic contaminations from turning was not performed.

2.2. Compaction

In order to create a uniform starting material and to facilitate the handling, approximately ten grams of aluminum chips were compacted in a single-acting press. Depending on the compressional forces (F_c), pre-compacts of 12 to 15 mm in height and a diameter of 20 millimeters were produced. As compacts with lower densities are assumed to support local heating and allow some extra deformation during the PECS process, specimens are compacted with pressures (σ_c) of 160, 320, 480, 640, 800 and 960 MPa to examine the influence of differences in green compact density.

2.3. Consolidation

To examine the bonding behavior of chip-based specimens under elevated pressure and temperature during current flow, two systems were chosen. Figure 4 shows the schematic tool assembly for PECS using the Gleeble systems standard clamping jaws to transmit the current flow over the dies and specimen. While the right side of the assembly is fixed, the left side is displaceable to apply mechanical force to the specimens. In order to prevent the clamping jaws from slipping backwards under compressive stress, not illustrated adjustable steel brackets are used to hold them in place. To examine the influence of die conductivity two interchangeable sets of tools, one being machined from Q & T steel 42CrMo4 and the other one from copper alloy CuCr1Zr are used during experiments. Additionally, a mixture of both tool sets with copper punches and steel container is used during processing. Two type K thermocouples are used to monitor and control the sintering process, as the Gleeble systems power input is controlled via target temperature (P-Temp) values. Based on the system used, the amount of current applied cannot be controlled specifically. While TC3 is used to control the preset target temperature, TC2 is used for monitoring only, as the positioning of the thermocouple close to the inner wall of the container resulted in a less stable behavior of the temperature reading. As this setup results in a thermal hotspot at the assembly center, TC2 is used to monitor the specimen temperature. It is essential to ensure a peak temperature around 500 °C is not surpassed during experiments to reduce the risk of damaging the copper tools due to thermal softening. In preliminary investigations with this setup, an ON/OFF pulse pattern of 480 cycles with 250/125 mm and an actuation time of one mm in between each step was developed. After a continuous heat up to 300 °C within 90 s, this pattern is applied to all specimens if not stated otherwise. A detailed summary of used processing parameters for specimens is given in Table 1. Regarding specimens labeling, C denotes usage of the copper container and S denotes usage of the steel container during processing. During heat up and the first 240 cycles of pulsing, only low pressure is applied to ensure contact between punches and specimens and to enhance micro-arc welding. To facilitate bonding,

higher pressure is applied during a pulsing break of 5 s and kept constant for the concluding 240 cycles. Additional deformation at elevated temperature promotes oxide breakage caused by a wider spread between the hardness values of base metal and the brittle surface oxide [15,30]. Therefore, all specimens, except C-1, S-1 and both SPS specimens, are sintered using delayed pressure application. The SPS setup with a graphite tool assembly is used to produce reference specimens with a processing temperature of 550 °C and a maximum sintering pressure (σ_s) of 51 MPa. As shown in Figure 5, specimens are heated to 550 °C within 10 minutes, followed by one minute of holding at peak temperature and a controlled cooling step towards 400 °C within one minute. As a further increase in temperature and compressive force lead to breakage of graphite die components, only the way of pressure application is varied. Specimen SPS-1 is pressurized with 51 MPa before current application and kept constant during processing, while SPS-2 was linearly loaded from 16 to 51 MPa simultaneously with temperature arising between 400 to 550 °C.

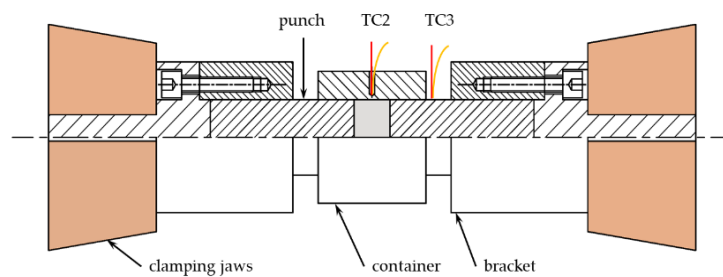


Figure 4. Tool assembly containing two punches and an interchangeable container, controlled via type K thermocouples during PECS experiments on the Gleeble 3800 system.

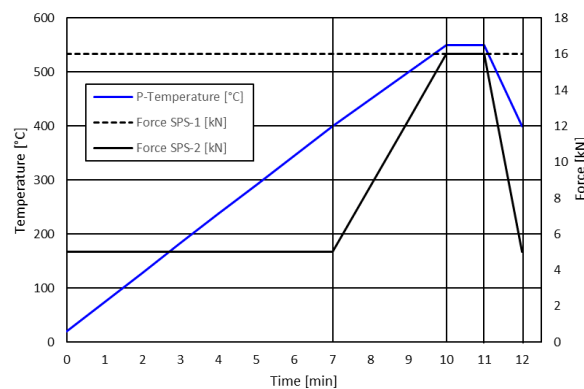


Figure 5. Preset temperature and pressure curves used during fabrication of reference spark plasma sintering (SPS) specimens with a maximum load of 16 kN, equaling an applied pressure of 51 MPa.

Table 1. Relevant parameters used during fabrication of the evaluated specimens for this research. SPS-1 and SPS-2 are specimens produced on the reference system.

Sample	F_c [kN]	σ_c [MPa]	Punch	Die	F_s [kN]	σ_s [MPa]	P-Temp [°C]
SPS-1	250 < F_c < 300	800 < σ_c < 960	Graphite	Graphite	16 **	51 **	550
SPS-2	250 < F_c < 300	800 < σ_c < 960	Graphite	Graphite	16 ** (r)	51 ** (r)	550
C-1	250 < F_c < 300	800 < σ_c < 960	Copper	Copper	5 **	16 **	300/350
S-1	250 < F_c < 300	800 < σ_c < 960	Copper	Steel	5 **	16 **	300/350
C-2	250 < F_c < 300	800 < σ_c < 960	Copper	Copper	5/15 *	16/48 *	300/350
S-2	250 < F_c < 300	800 < σ_c < 960	Copper	Steel	5/15 *	16/48 *	300/350
C-3	250 < F_c < 300	800 < σ_c < 960	Copper	Copper	5/20 *	16/64 *	300/350
S-3	250 < F_c < 300	800 < σ_c < 960	Copper	Steel	5/20 *	16/64 **	300/350
C-4	250 < F_c < 300	800 < σ_c < 960	Copper	Copper	5/20 *	16/64 *	350/400
S-4	250 < F_c < 300	800 < σ_c < 960	Copper	Steel	5/20 *	16/64 *	350/400
C-5	200	640	Copper	Copper	5/20 *	16/64 *	350/400
S-5	200	640	Copper	Steel	5/20 *	16/64 *	350/400
C-6	150	480	Copper	Copper	5/20 *	16/64 *	350/400
S-6	150	480	Copper	Steel	5/20 *	16/64 *	350/400
C-7	100	320	Copper	Copper	5/20 *	16/64 *	350/400
S-7	100	320	Copper	Steel	5/20 *	16/64 *	350/400
C-8	50	160	Copper	Copper	5/20 *	16/64 *	350/400
S-8	50	160	Copper	Steel	5/20 *	16/64 *	350/400

(r)—linear ramp up simultaneous to temperature increase. **—constant force application during sintering. *—delayed force application with initial pressure/pressure after pulsing break.

2.4. Evaluation

For comparison among the specimens metallographic examination of their densities, hardness and structures are executed after cutting them in half. Sample densities were calculated from measurements using digital scale and digital caliper with tolerances of ± 0.01 mm and ± 0.01 g, as the Archimedes method is considered problematic for structures with residue open porosity. It would lead to overestimation during density measurements and entrapped fluids after weighing would possibly cause voids during further processing [31,32]. The polished samples are observed with an Olympus BS53M light optical microscope prior and after hardness measurements. Vickers micro-hardness HV0.5 is measured on an EMCOTEST M1C 010 hardness tester, using the same schematic pattern for all specimens, shown in Figure 6. To enable comparability amongst samples with different thermal histories and to bulk reference material, the second half of promising specimens were brought to T6 temper by solution annealing at 530 °C and artificial ageing at 170 °C, as heat treatment leads to desired material structure in 6xxx aluminum alloys.

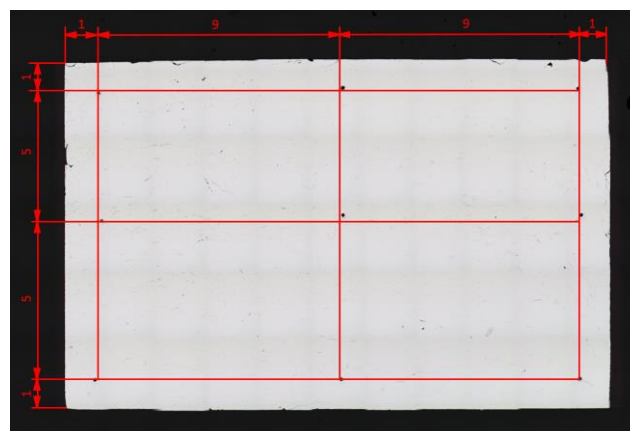


Figure 6. Schematic pattern used during hardness measurements to evaluate PECS specimens with distances between indents in millimeters.

3. Results

Figure 7 shows results of all individual processing steps with (a) chips after comminution, cleansing and evaluation via pyrolysis, (b) a briquette after pre-compaction with a load of approximately 320 MPa and (c) a finished specimen consolidated via PECS on the thermomechanical treatment simulator Gleeble 3800. In the following subsections, the results from compaction and consolidation will be discussed in detail.

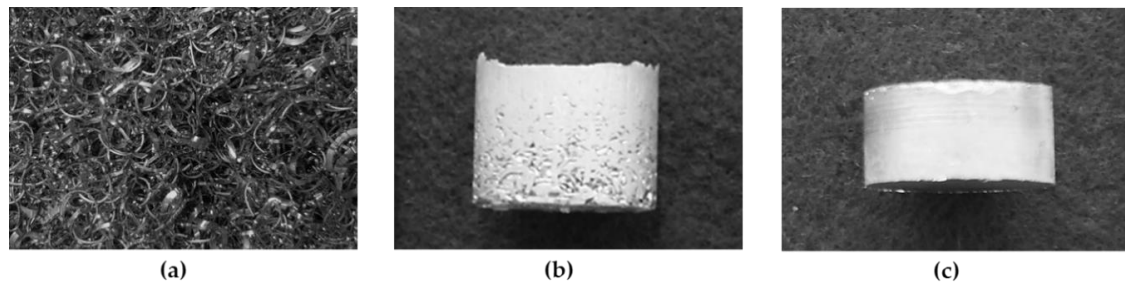


Figure 7. Aluminum EN AW 6082 specimens for experimental procedure after (a) comminution and cleansing, (b) compaction in a single-acting hydraulic press and (c) consolidation via PECS in a Gleeble 3800 system.

3.1. Compaction

Based on the low bulk densities of loose chips, volume of compacts reduces to about one-sixth during compaction with pressures around 960 MPa and final densities of about 2.7 g/cm^3 are reached. Figure 8 shows the quite significant optical differences between briquettes, caused by compression with 160 to 960 MPa. Specimens compacted with pressures around 800 MPa show no significant or measurable difference in size and density to briquettes produced with 960 MPa. Therefore, all specimens compressed above 800 MPa are presumed to be almost identical base material for the following consolidation processes. During sample preparation, all irregular excess material, caused by tolerances and wear between punch and die, is removed prior to further processing. Due to the single-acting press, particles close to the moving punch of the compaction device experience higher relative movement and therefore higher deformation during pressing. This results in a clearly visible density gradient from top to bottom of the specimens. Figure 9 shows a briquette compacted with a pressure around 960 MPa, exhibiting an increased number of cracks towards the lower, not moving surface and a denser upper side. Despite the high compression, chips only show interlocking connections after briquetting, with gaps and cracks between chips been clearly apparent under the microscope. Nevertheless, bonding between the single particles is strong enough to allow geometrical adaptations on a conventional lathe after a compression above 640 MPa.

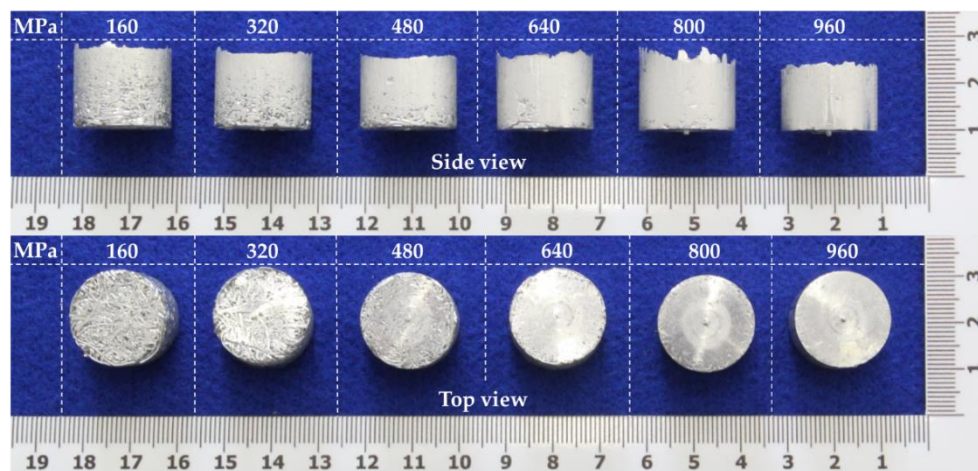


Figure 8. Side and top view of aluminum chips showing different compact densities caused by the variation of briquetting pressures between 160 and 960 MPa.

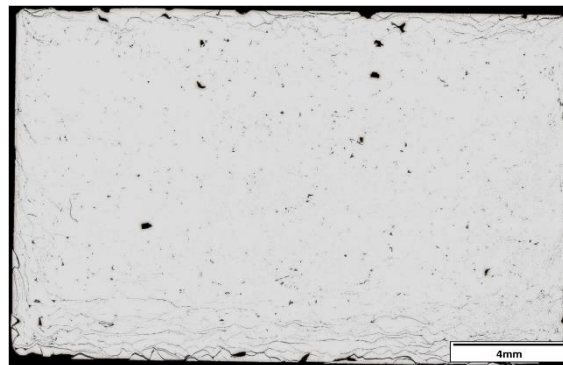


Figure 9. Chip-based aluminum briquette after a compression with 960 MPa in a single-acting hydraulic press, magnification factor $\times 50$.

3.2. Pulsed Electric Current Sintering

During processing on the Gleeble system, temperature, stroke and power angle are especially monitored to gain information about process stability. Figure 10 gives an exemplary overview on controlling and monitoring parameters during PECS, with target temperature, compressive force and time being the main input parameters and a possible evaluation of results via measured temperatures and stroke movement. Process data recorded during sintering of specimen C-4 clearly shows a difference between target and actual temperature during pulsing. This behavior is known from preliminary experiments and target program temperature is set accordingly, to achieve systems maximum power input available during pulsing, while staying within a maximum temperature of 500 °C for measurements at TC2. After a pulsing pause during load application, even maximum system power is not able to provide same temperature levels as prior to pressure application, regardless of the tool material used. This may be attributed to a lack in system power available or result from higher conductivity within the assembly through the additional compression of voids inside the specimen. Even though all samples show similar temperature behavior, this drop is more pronounced for experiments using the copper container, especially for temperature readings on TC2. Based on the higher conductivity and thermal reactivity, the copper container additionally results in higher temperature peaks at the beginning of the process. A comparison of those temperature readings, to measurements of experiments using same parameters in combination with a steel container, is displayed in Figure 11. Comparison of temperature curves reveals, only the combination of steel container and pre-compacts pressurized above 800 MPa achieves a temperature increase after pulsing

break. For both steel and copper container, specimen number C-5 and S-5 record the highest temperature readings during processing. This may be attributed to a higher number of voids within the specimens compressed at 640 MPa, leading to higher electrical resistance and therefore higher resulting temperatures through resistance heating. A further decrease in pre-compact density results in a clear drop in temperature, indicating a more pronounced current flow over the container, possibly caused by resistivity reaching a threshold. As current flow over the specimen further decreases, the tool assemblies are mainly heated according to the conductivity of each tool material. Therefore, especially the copper container suffers a significant temperature drop. Differences for specimens C-7 and S-7, trending towards C-6 with the copper container and towards S-8 in the steel container, are attributed to load fluctuations during compaction. Comparisons to punch stroke during PECS presented in Figure 12, confirm specimen C-7 being pre-compressed with higher load than specimen S-7, as all other curves are almost identical for both tool assemblies. For dense samples pre-compacted with pressures above 640 MPa, thermal expansion is higher than densification during application of maximum pressure during PECS. Based on this observation, applied pressure is too low to result in significant densification compared to pre-pressed state for these specimens. Pre-compacts with 480 MPa and below are showing a less pronounced thermal expansion within tool assembly and significant compression of the specimen during processing. Therefore, considerable improvements in sample density are only expected for less compressed pre-compacts, showing punch movement exceeding the movement caused by thermal expansion during heat up. Additional, similarities between stroke curves of both assemblies indicate almost identical thermal states of compacts inside the tools while PECS, independent of the container material.

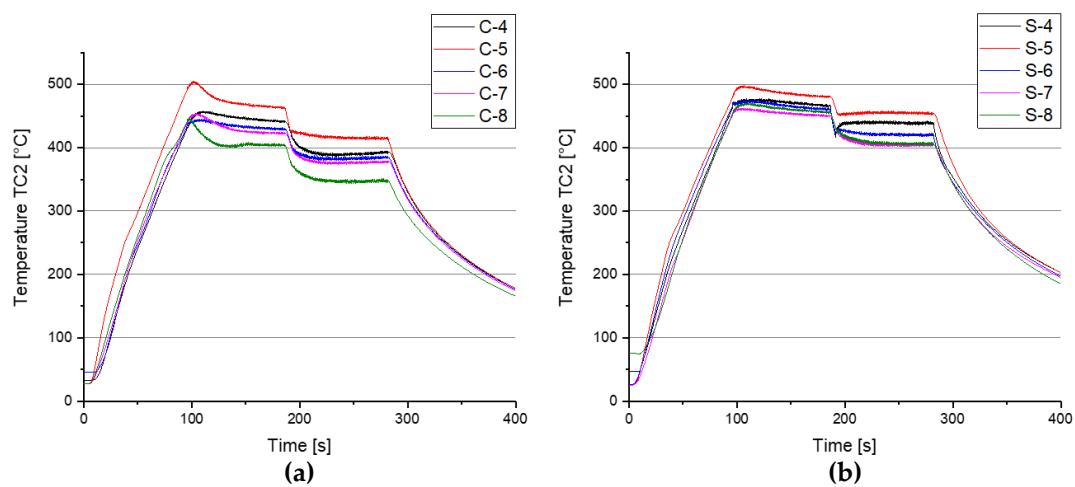


Figure 10. Temperature readings of TC2 during processing within the Gleeble 3800 system of specimens for all tested densities in (a) copper container and (b) steel container.

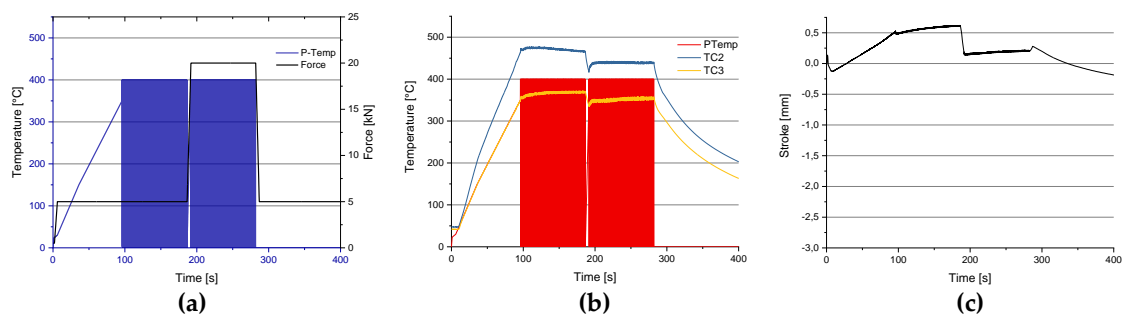


Figure 11. Exemplary parameters during PECS of specimen C-4 with delayed force application in a Gleeble 3800 thermomechanical treatment simulator for preset inputs (a) force and target temperature over time and during processing for (b) temperature and (c) stroke over time.

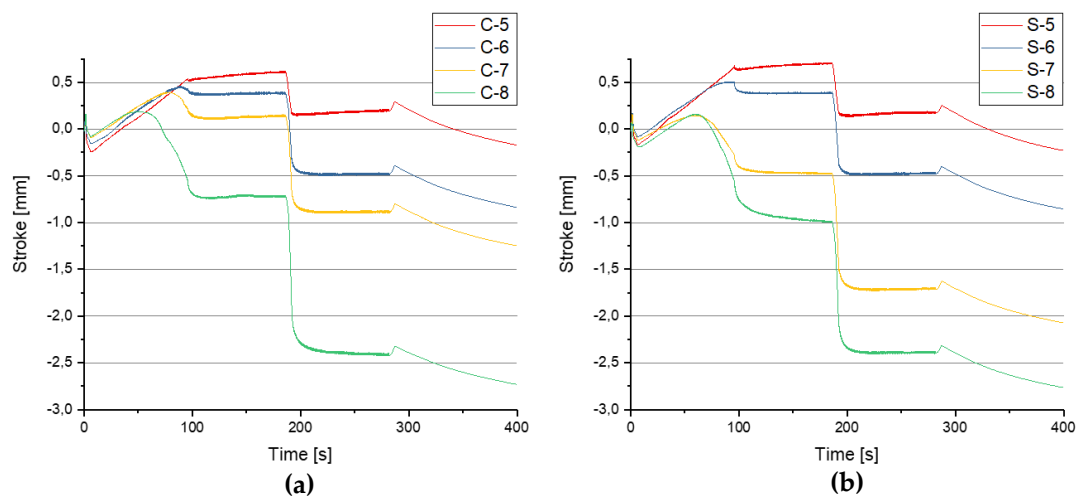


Figure 12. Comparison of stroke during PECS with different tool assemblies for specimens (a) C-5 to C-8 and (b) S-5 to S-8 with C-4 and S-4 being excluded for being almost identical to C-5 and S-5.

3.2.1. Density Measurements

Due to the unknown amount of oxides surrounding the chips, different opinions on the actual amount of oxides on chip-based compacts are presented in recent literature. Therefore, relative densities were determined according to two individual absolute densities, to show both upper and lower end of estimations regarding final specimen densities achieved. While Behrens et al. [33] used 2.71 g/cm³ for their calculations on Al EN AW 6082 chips, Paraskevas et al. [24] reported of fully dense samples of the same alloy reaching 2.832 g/cm³, indicating a much higher amount of oxides. Evaluation of specimens described in this work, based on measurements of the individual samples and calculated relative densities for both above stated cases, is presented in Table 2. As previously assumed based on machine data, specimens pre-pressed with 640 MPa and above, show similar densities prior to and after sintering, with only minor variation in density. Additionally, SPS specimens show similar densities like samples produced on the Gleeble system. For briquettes pre-compacted with a pressure of 480 MPa and below, compression during sintering leads to a significant increase in final density compared to pre-compaction. Except specimens compacted with 160 MPa, all other samples reach relative densities either around 99% compared to 2.71 g/cm³ or 95% if compared to a reference density of 2.832 g/cm³. Since the oxide content within the specimens is not known, these calculated values may only serve as an orientation. Nevertheless, they clearly indicate that no produced specimen reaches full relative density and residue porosity has to be expected during optical evaluation.

Table 2. Measured densities after pre-compaction (ρ_c) and sintering (ρ), with calculated relative densities based on reports, suggesting a final density of 2.71 kg/cm³ [33] and 2.832 kg/cm³ [24] for chip-based specimens.

	σ_C [MPa]	ρ_c [g/cm ³]	ρ [g/cm ³]	ρ_{C1} [%]	ρ_1 [%]	ρ_{C2} [%]	ρ_2 [%]
		Measurements		$\rho_{6082} = 2.71$		$\rho_{6082} = 2.832$	
SPS	>800	2.662	2.673	98.23	98.63	94.00	94.39
	>800	2.670	2.705	98.52	99.82	94.28	95.52
PECS	640	2.663	2.695	98.27	99.45	94.03	95.16
	480	2.513	2.698	92.73	99.56	88.74	95.27
	320	2.375	2.692	87.64	99.34	83.86	95.06
	160	2.172	2.651	80.15	97.82	76.69	93.61

3.2.2. Light Optical Microscopy

To further examine the bonding between chips, the cross sections and some highlights of representative regions amongst all PECS specimens in comparison to results from SPS are presented subsequently. During optical evaluation, main focus is concentrated towards specimens produced with highest pressures during sintering. As shown in Figure 13a, lower pressure of 16 MPa during PECS results in less dense samples, with little optical improvement compared to cold-pressed briquettes. The other samples pictured in Figure 13, exhibit less voids between single particles and a more homogeneous structure throughout the whole cross section. This can be attributed to the increased processing pressure of 64 MPa for PECS and 51 MPa for SPS samples. Even though sintered with a lower pressure of 51 MPa, the cross section of specimen SPS-1 reaches the optical most homogeneous structure with the least number of voids visible. Most probably, this is caused by the elevated processing temperatures and a consequently reduced yield stress of the aluminum alloy at this configuration, allowing higher deformation even with less pressure applied. Depending on the position observed under the microscope, residue chip boundaries are clearly visible within all specimens at higher magnification, like those displayed in Figure 14a,c. Pre-compaction leads to an inhomogeneous structure within briquettes caused by the single-acting hydraulic press and the related differences in relative movement within the cross section. Therefore, less deformed regions tend to show minor bonding with visible chip boundaries after sintering. Nevertheless, regions being higher deformed after pre-compaction, like shown in Figure 14b,d, exhibit little to no residue boundaries apparent after sintering, proofing the bonding potential for chip-based samples via PECS/SPS. While some of these well-bonded areas exhibit a defect free microstructure, some of the regions still show interrupted boundaries enabling identification of preceding chip structure under the microscope, visible in Figure 15a. The visible boundaries indicate only partial bonding amongst chips through necking and incomplete dispersion of the surface layer into the microstructure. Even though specimen SPS-1 is the most homogeneous specimen, these residue structures may result in reduced mechanical properties through a reduced bonding surface. Throughout PECS specimens, exemplary pictured in Figure 15b,c, bonding seems to be superior within well-bonded regions, but inhomogeneity is higher within the cross-section, if compared to SPS samples. These differences in bonding may result from holding time at peak temperature being tripled for PECS referred to SPS. For PECS, specimens pre-compacted with less than 640 MPa resulted in reduced density with an increased number of voids within the cross-section, when using the cooper container. Attributed to the lower processing temperatures, this assembly shows an increased sensitivity towards pre-compact density. For specimens produced with the steel container, this drop in density was only noticeable for briquettes pre-compacted with 320 MPa and below, indicating a more pronounced influence of the current, when using less conductive containers. Correlating higher temperatures allow higher compression even for same loads applied and therefore result in denser specimens. Like visible in Figures 14b and 15c, the microstructure of specimen C-3 indicates a decrease in temperature dependence, when sintering high-density pre-compacts, further emphasizing the positive effect of current application on bond formation. Regardless of the system and tool material, sintered specimens show improved bonding and disrupted chip boundaries in some areas after current application. Therefore, a clear statement on the effects responsible for consolidation is not possible and may be considered a combination of current, deformation and temperature.

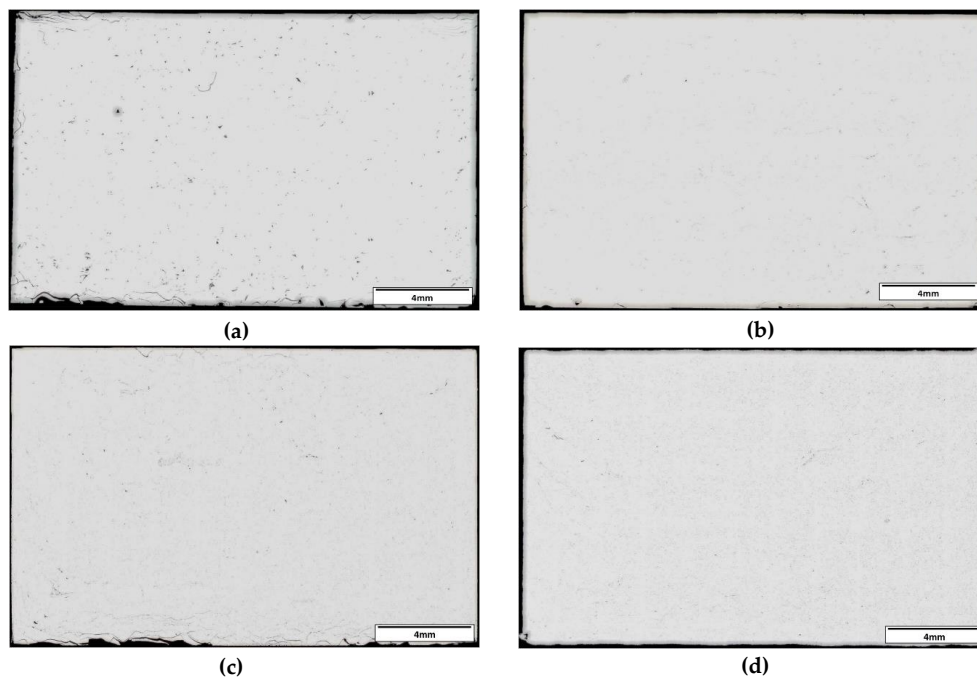


Figure 13. Light optical microscopy images showing variations in sample density depending on processing parameters and systems used for specimens (a) S-1, (b) S-6 and (c) C-3 produced on the Gleeble system and (d) SPS-1 from the reference system, magnification factor $\times 50$.

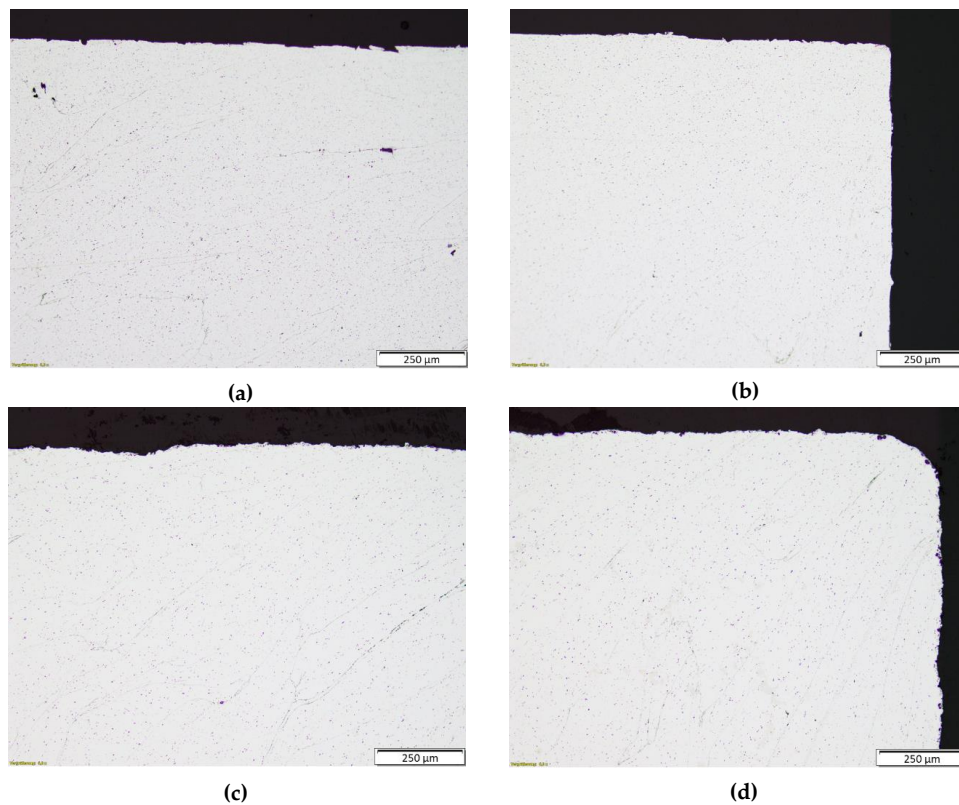


Figure 14. Light optical microscopy images with similar bonding between specimens in most homogeneous regions towards their outer diameter with pictures (a) and (b) showing C-3 and (c) and (d) showing SPS-1. While (a) and (c), taken on the outer edge towards the center of specimens height, still exhibit visual chip boundaries, (b) and (d) show specimens most deformed regions towards the corners, with little to no chip boundaries visible, magnification factor $\times 100$.

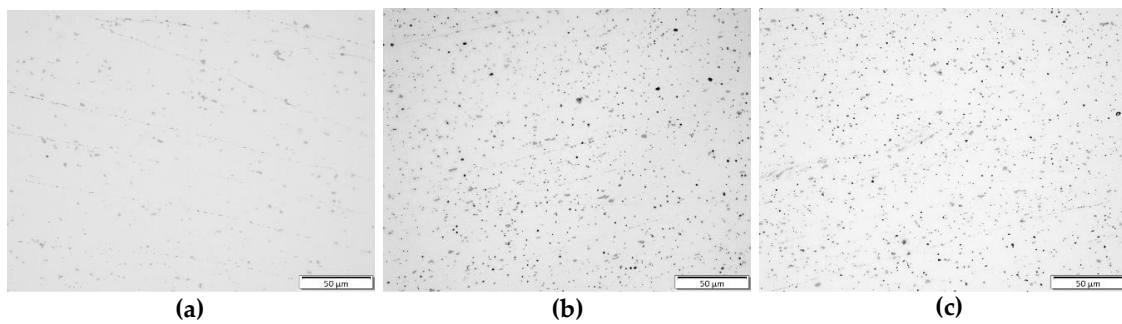


Figure 15. Light optical microscopy images of specimens (a) SPS-1, (b) C-6 and (c) C-3 with good bonding and only little residue chip boundaries visible in specimens most deformed regions, magnification factor $\times 500$.

3.2.3. Hardness Measurements

Vickers micro-hardness measurements are performed with the same pattern applied for all specimens produced, to evaluate most characteristic positions in all samples. Figure 16 shows the microscopy images of characteristic hardness indents within samples after experiencing different treatments, with (a) being pre-compacted only, (b) being sintered with PECS and (c) being sintered with SPS. While indents show very irregular shapes and delamination in chip-based briquettes after compaction when positioned close to chip boundaries, indents in sintered specimens, regardless of the system used, do not show this behavior. Even samples produced during calibration of the tool assembly exhibit elevated bonding amongst individual chips compared to the solely interlocking connections in the pre-compacts and therefore proof a bonding effect of PECS. As temperatures differ during processing due to the variation of setups, a direct comparison of hardness values without further treatment leads to high fluctuations amongst individual samples. Therefore, samples produced with PECS result in lower hardness compared to specimens produced via SPS. Due to the highly conductive graphite die and elevated temperature during sintering, intermetallic Mg_2Si is dissolved while PECS and faster cooling rates limit new precipitation to lower amounts, as can be seen in Figure 14. A reduced number of dark Mg_2Si phases is visible under the microscope for samples produced with SPS. To achieve better comparability, most representative specimens from preliminary investigations, PECS on the Gleeble system and SPS are homogenized by solution heat treatment. Summarized Vickers micro-hardness measurements are presented in Table 3. Specimens T-1 and T-2 are produced in an initial tool assembly using the Q & T steel 42CrMo4 without any copper elements. While no container nor an additional pulse sequence were used during preliminary investigations on the Gleeble system, samples T-1, T-2 are produced by similar parameters to other evaluated specimens with only pulsing temperature being increased to 420 °C. Based on higher temperatures during processing, both of those specimens experienced higher deformation than others fabricated. Hardness measurements after heat treatment show similar results amongst all experiments, with the highest values in samples from preliminary experiments even surpassing those from the designated SPS system. Average values of up to 116 HV0.5 are just below measurements taken from commercial Al EN AW 6082 bars averaging at about 118 HV0.5 [26]. Even with maximum values reaching comparable levels as reference material, high standard deviation within specimens reflects inhomogeneities throughout the cross section. Through inhomogeneous consolidation of the chips, heat treatment results in delamination and crack propagation within specimens caused by entrapped and pressurized air [26]. In combination with lowered material strength and a thermal expansion of the air, even specimens rated as well-bonded prior to heat treatment suffer from crack propagation, as can be seen in Figure 17. Generally speaking, specimens produced at higher temperatures show less delamination after heat treatment, with a high influence resulting from additional deformation during current application. As specimen T-1 was heated to almost 500 °C during calibration, even low pressure applied causes high deformation, upsetting the sample from twelve to four millimeters in height during sintering. An increase in

hardness difference between oxides and base metal results in higher oxide breakdown and therefore facilitates metal bonding [30]. This combination of additional forging and the current applied results in the least amount of delamination and highest hardness values after heat treatment for specimen T-1, as displayed in Figure 18. Due to the small punch diameters, a delamination of the specimen around the outside during upsetting cannot be prevented. An undefined pressure state towards specimens boundaries again causes relatively high standard deviation for this promising specimen. Therefore, a different tool assembly would be necessary to ensure constant contact and pressure application during higher deformation. Again, consolidation within the specimen needs to be attributed to more than one effect, but clearly indicates the importance of high deformation under elevated temperature.

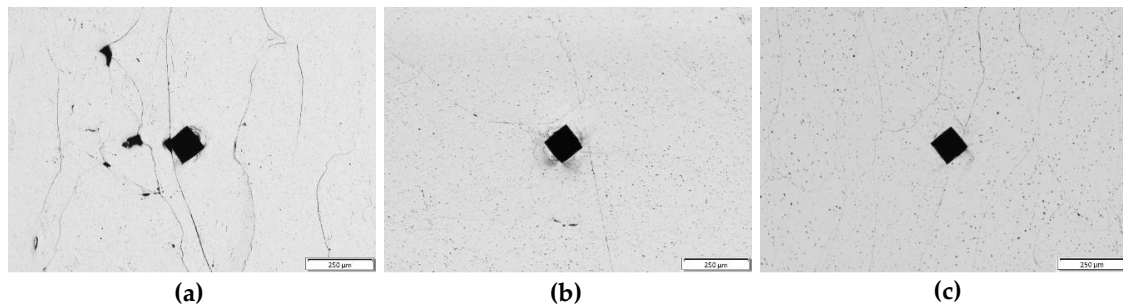


Figure 16. Characteristic hardness indents close to chip boundaries from HV0.5 Vickers micro-hardness measurements on specimens after (a) cold-pressing, (b) sintering on the Gleeble system and (c) sintering on the SPS-system, with clear delamination only visible for briquettes prior to sintering.

Table 3. Comparison amongst specimens in as sintered and T6 tempered state via HV0.5 Vickers micro-hardness measurements including standard deviation (σ) within samples.

Sample	\varnothing	as sintered			σ	T6 temper		
		min.	max.	σ		\varnothing	min.	max.
T-1	42.7	37.8	44.3	1.1	113.7	106	123	5.6
T-2	41.6	35.9	49.5	2.8	116.1	108	121	4.1
C-3	39.0	35.0	42.8	2.1	110.6	101	114	3.7
S-6	44.6	40.8	56.9	4.7	107.6	91.7	120	9.7
SPS-1	60.7	58.8	62.4	1.0	110.6	94.0	118	7.5
SPS-2	59.8	55.3	63.2	2.1	111.7	102	119	5.6

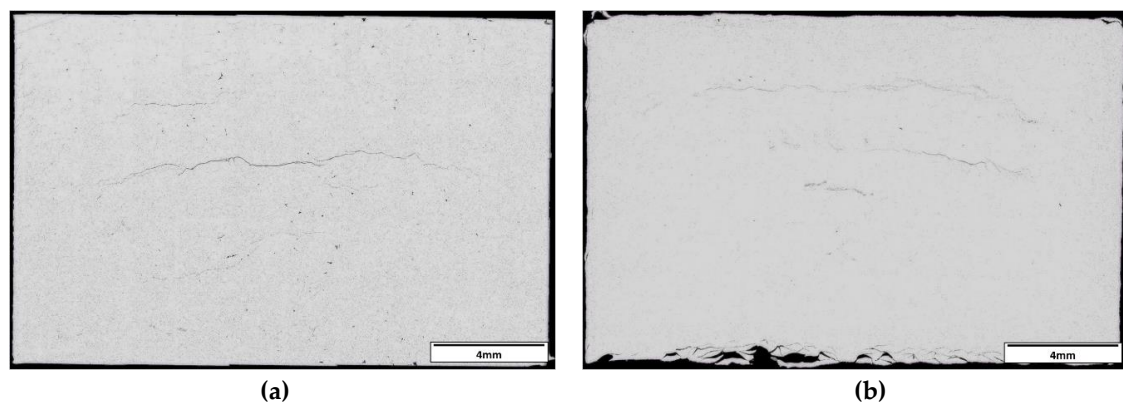


Figure 17. Light optical microscopy images showing delamination after heat treatment for optical well bonded samples (a) S-6 and (b) SPS-1, magnification factor $\times 50$.

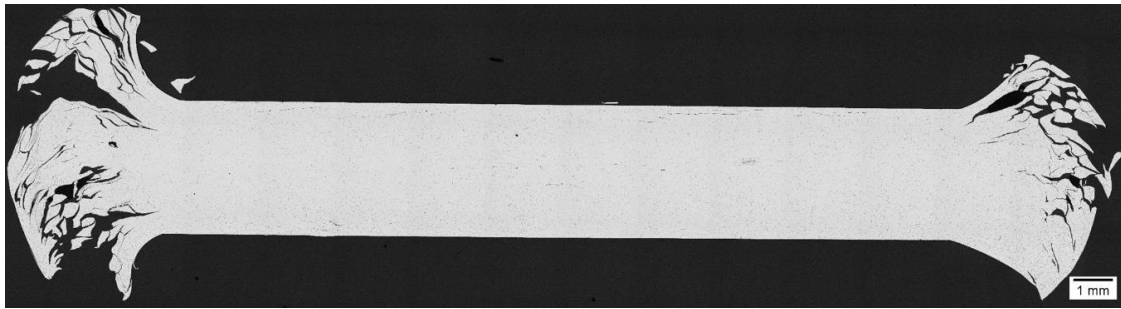


Figure 18. Light optical microscopy image showing specimen T-1 from preliminary calibrations with excessive deformation due to elevated processing temperatures with no significant delamination after heat treatment, magnification factor $\times 50$.

4. Discussion

Even though all specimens produced show areas with inhomogeneous results with some unbonded regions, a positive effect of PECS on the consolidation behavior of chip-based briquettes is clearly visible. Compared to initial briquettes, optical improvements as well as measurable improvements in density and hardness are achieved for all samples produced.

Unfortunately, bonding quality throughout specimens is not uniform, resulting in partial delamination during heat treatment originating from these less bonded regions. Based on the one-sided moving hydraulic press used for pre-compaction of the briquettes, starting material shows inhomogeneous deformation prior to sintering experiments and needs further optimization to create a more uniform starting material. Due to high pressures used during pre-pressing of the chips to facilitate the handling during experiments, pressurized air gets entrapped within specimens. Elevated temperatures during solution annealing therefore cause expansion of those gases initiating crack growth throughout the thermally softened material.

As a variation of the container material showed no significant effects on bonding quality and the less conductive steel container results in more constant temperatures, this less temperature sensitive material combination seems to be the appropriate material combination. The insulating container results in less current surpassing the sample and force the current flow over the specimen. In addition, the steel container is able to handle higher compressive forces to allow higher degrees of deformation. As differences amongst specimens pre-compacted with pressures between 480 MPa and 960 MPa did not show significant variations in final density after sintering, 640 MPa is found to be most appropriate for PECS by achieving highest processing temperatures at TC2 and enabling additional deformation during load application. Increased pressure along with higher processing temperatures during pulsed electric current sintering increases available free energy and facilitates diffusion, leading to enhanced bonding, as clearly indicated by results of this work. Additionally, less air will be entrapped within the briquettes at lower compacting pressures and a reduced amount of delamination can be expected during heat treatment.

To enable a successful implementation of solid state recycling, the consolidation process as well as PECS processing parameters provide potential to be further optimized. If residue porosity, non-uniform bonding and entrapped air are still problematic after optimization of processing parameters, combinations with metal forming processes like upsetting may help to produce void-free specimens. Collection and preparation of the contaminated chips have to be considered for industrial implementation, as contaminations with other aluminum alloys are not compensable and individual separation steps to eliminate impurities of any kind result in higher processing costs. Once sorted and cleaned properly, storage and handling without further pollution is essential. Compaction of the chips is more difficult without lubrication and results in adhesion between aluminum and tools with high abrasive wear. Nevertheless, pulsed electric current sintering may be considered as a very interesting and promising alternative to conventional solid-state recycling approaches for aluminum.

5. Conclusions and Outlook

- Sorting, storage and cleansing of the chips is a key factor for successful solid state recycling, to prevent impurities and enable metallic bonding.
- PECS achieves optical as well as measurable improvements in density and hardness compared to only pre-compacted briquettes specimens proving more superior bonding after sintering.
- Final density of specimens pre-compacted above 320 MPa reaches similar levels after sintering even with different systems used.
- Increased temperature, pressure and therefore deformation result in higher quality bonding amongst individual chips.
- Inhomogeneity within specimens due to the chips morphology and the pre-compaction process lead to a partial delamination of the chips during heat treatment.

Even though this work proves a positive influence of PECS on the consolidation behavior of aluminum chips, further work will be necessary to achieve homogenous bonding throughout specimens required for an industrial application:

- Pre-compaction should be carried out on double-acting presses to prevent a density gradient within the briquettes and leading to a more homogenous starting material, enabling more uniform consolidation during PECS.
- Further optimization of process parameters may deliver a more suitable processing cycle, leading to superior bonding and desired material properties, and possibly preventing delamination effects.
- A combination of PECS with a deformation-based process may be used to additionally enhance bonding.

Author Contributions: C.N.C. and B.K. designed and carried out experiments, analyzed results and wrote the paper. B.B. and C.W. provided general guidance and proofread the manuscript writing. All authors have read and agreed to the published version of the manuscript.

Funding: This research received no external funding.

Acknowledgments: The authors want to thank Alexander Wimmer and Neuman Aluminium GmbH, located in Marktl, Austria, for providing the EN AW 6082 chips, used for this research work.

Conflicts of Interest: The authors declare no conflict of interest.

References

1. Paraskevas, D.; Kellens, K.; Dewulf, W.; Duflou, J.R. Environmental modelling of aluminium recycling: A Life Cycle Assessment tool for sustainable metal management. *J. Clean. Prod.* **2015**, *105*, 357–370. [[CrossRef](#)]
2. Rombach, G. Raw material supply by aluminium recycling—Efficiency evaluation and long-term availability. *Acta Mater.* **2013**, *61*, 1012–1020. [[CrossRef](#)]
3. Castro, M.B.G.; Remmerswaal, J.A.M.; Reuter, M.A.; Boin, U.J.M. A thermodynamic approach to the compatibility of materials combinations for recycling. *Resour. Conserv. Recycl.* **2004**, *43*, 1–19. [[CrossRef](#)]
4. Amini, S.H.; Remmerswaal, J.A.M.; Castro, M.B.G.; Reuter, M.A. Quantifying the quality loss and resource efficiency of recycling by means of exergy analysis. *J. Clean. Prod.* **2007**, *15*, 907–913. [[CrossRef](#)]
5. Nakamura, S.; Kondo, Y.; Matsubae, K.; Nakajima, K.; Tasaki, T.; Nagasaka, T. Quality- and dilution losses in the recycling of ferrous materials from end-of-life passenger cars: Input-output analysis under explicit consideration of scrap quality. *Environ. Sci. Technol.* **2012**, *46*, 9266–9273. [[CrossRef](#)] [[PubMed](#)]
6. Cislo, C.N.; Fazokas, T.; Buchmayr, B.; Weiß, C. Prozessanalyse zum ressourcenschonenden Recycling von Spanschrotten aus der Aluminiumverarbeitung. In *Konferenzband zur 14. Recy & DepoTech-Konferenz: Recycling & Abfallverwertung, Abfallwirtschaft & Ressourcenmanagement Sowie Deponietechnik & Altlasten*; Eigenverlag des Lehrstuhls für Abfallverwertungstechnik & Abfallwirtschaft: Leoben, Austria, 2018; pp. 231–238.
7. Duflou, J.R.; Tekkaya, A.E.; Haase, M.; Welo, T.; Vanmeensel, K.; Kellens, K.; Dewulf, W.; Paraskevas, D. Environmental assessment of solid state recycling routes for aluminium alloys: Can solid state processes significantly reduce the environmental impact of aluminium recycling? *Cirp Ann.-Manuf. Technol.* **2015**, *64*, 37–40. [[CrossRef](#)]

8. Gronostajski, J.Z.; Kaczmar, J.W.; Marciniak, H.; Matuszak, A. Direct recycling of aluminium chips into extruded products. *Achiev. Mech. Mater. Eng.* **1997**, *64*, 149–156. [[CrossRef](#)]
9. Shamsudin, S.; Lajis, M.A.; Zhong, Z.W. Solid-state recycling of light metals: A review. *Adv. Mech. Eng.* **2016**, *8*, 1–23. [[CrossRef](#)]
10. Wan, B.; Chena, W.; Lua, T.; Liua, F.; Jianga, Z.; Maoa, M. Review of solid state recycling of aluminum chips. *Resour. Conserv. Recycl.* **2017**, *125*, 37–47. [[CrossRef](#)]
11. Munir, Z.A.; Quach, D.V.; Ohyanagi, M. Electric Current Activation of Sintering: A Review of the Pulsed Electric Current Sintering Process. *J. Am. Ceram. Soc.* **2011**, *94*, 1–19. [[CrossRef](#)]
12. Munir, Z.A.; Quach, D.V.; Ohyanagi, M. The effect of electric field and pressure on the synthesis and consolidation of materials: A review of the spark plasma sintering method. *J. Mater. Sci.* **2006**, *41*, 763–777. [[CrossRef](#)]
13. Rahaman, M.N.B. *Ceramic Processing and Sintering*; Marcel Dekker Verlag: New York, NY, USA, 1995; Volume 33, pp. 425–539.
14. Guillon, O.; Gonzalez-Julian, J.; Dargatz, B.; Kessel, T.; Schiering, G.; Räthel, J.; Herrmann, M. Field-Assisted Sintering Technology/Spark Plasma Sintering: Mechanisms, Materials, and Technology Developments. *Adv. Eng. Mater.* **2014**, *16*, 830–849. [[CrossRef](#)]
15. Dong, P.; Wang, Z.; Wang, W.; Chena, S.; Zhou, J. Understanding the spark plasma sintering from the view of materials joining. *Scr. Mater.* **2016**, *123*, 118–121. [[CrossRef](#)]
16. Locci, A.M.; Cincotti, A.; Todde, S.; Orrù, R.; Cao, G. A methodology to investigate the intrinsic effect of the pulsed electric current during the spark plasma sintering of electrically conductive powders. *Sci. Technol. Adv. Mater.* **2010**, *11*, 045005. [[CrossRef](#)]
17. Chen, W.; Anselmi-Tamburini, U.; Garay, J.E.; Groza, J.R.; Munir, Z.A. Fundamental investigations on the spark plasma sintering/synthesis process. *Mater. Sci. Eng. A* **2005**, *394*, 132–138. [[CrossRef](#)]
18. Kellogg, F.; McWilliams, B.; Cho, K. Effect of Current Pathways during Spark Plasma Sintering of an Aluminum Alloy Powder. *Metall. Mater. Trans. A* **2016**, *47*, 6353–6367. [[CrossRef](#)]
19. Vanmeensel, K.; Laptev, A.; Hennick, J.; Vleugels, J.; Van der Biest, O. Modelling of the temperature distribution during field assisted sintering. *Acta Mater.* **2005**, *53*, 4379–4388. [[CrossRef](#)]
20. Zhaohui, Z.; Fuchi, W.; Lin, W.; Shukui, L.; Osamu, S. Sintering mechanism of large-scale ultrafine-grained copper prepared by SPS method. *Mater. Lett.* **2008**, *62*, 3987–3990. [[CrossRef](#)]
21. Song, X.; Liu, X.; Zhang, J. Neck Formation and Self-Adjusting Mechanism of Neck Growth of Conducting Powders in Spark Plasma Sintering. *J. Am. Ceram. Soc.* **2006**, *89*, 494–500. [[CrossRef](#)]
22. Orrù, R.; Licheri, R.; Locci, A.M.; Cincotti, A.; Cao, G. Consolidation/synthesis of materials by electric current activated/assisted sintering. *Mater. Sci. Eng. R* **2009**, *63*, 127–287. [[CrossRef](#)]
23. Saunders, T.; Grasso, S.; Reece, M.J. Plasma formation during electric discharge (50 V) through conductive powder compacts. *J. Eur. Ceram. Soc.* **2015**, *35*, 871–877. [[CrossRef](#)]
24. Paraskevas, D.; Vanmeensel, K.; Vleugels, J.; Dewulf, W.; Deng, Y.; Duflou, J.R. Spark Plasma Sintering as a Solid-State Recycling Technique: The Case of Aluminum Alloy Scrap Consolidation. *Materials* **2014**, *7*, 5664–5687. [[CrossRef](#)] [[PubMed](#)]
25. Paraskevas, D.; Vanmeensel, K.; Vleugels, J.; Dewulf, W.; Duflou, J.R. The Use of Spark Plasma Sintering to Fabricate a Twophase Material from Blended Aluminium Alloy Scrap and Gas Atomized Powder. *Procedia Cirp* **2015**, *26*, 455–460. [[CrossRef](#)]
26. Cislo, C.N.; Fazokas, T.; Buchmayr, B.; Weiß, C. Consolidation behaviour of aluminium alloy machining chips during the high pressure torsion process. In Proceedings of the Conference Proceedings of XXXVIII. Verformungskundlichen Kolloquium, Zauchensee, Austria, 23–27 March 2019; pp. 114–119.
27. Milkereit, B. Kontinuierliche Zeit-Temperatur-Ausscheidungs-Diagramme von Al-Mg-Si-Legierungen. Ph.D. Thesis, University of Rostock, Rostock, Germany, 1 December 2010.
28. Sefrin, H.; Kiechle, A.; Walker, G.; Zielasko, W.; Freiler, C.; Thomas, F.; Palm, I.; Eisenblätter, G.; Stäbler, D.; Breuer, D.; et al. Bestimmung und Beurteilung von Emissionen bei der spanenden Metallbearbeitung mit Minimalmengenschmierung. *Gefahrst.-Reinhalt. Der Luft* **2003**, *63*, 417–424.
29. Smeltzer, W.W. Oxidation of Aluminum in the Temperature Range 400°–600 °C. *J. Electrochem. Soc.* **1956**, *103*, 209. [[CrossRef](#)]

30. Xie, G.; Ohashi, O.; Yamaguchi, N.; Song, M.; Mitsuishi, K.; Furuya, K.; Noda, T. Behavior of oxide film at the interface between particles in sintered Al powders by pulse electric-current sintering. *Metall. Mater. Trans. A* **2003**, *34*, 699–703. [[CrossRef](#)]
31. Spierings, A.B.; Schneider, M.; Eggenberger, R. Comparison of density measurement techniques for additive manufactured metallic parts. *Rapid Prototyp. J.* **2011**, *17*, 380–386. [[CrossRef](#)]
32. Bai, S.; Perevoshchikova, N.; Sha, Y.; Wu, X. The Effects of Selective Laser Melting Process Parameters on Relative Density of the AlSi10Mg Parts and Suitable Procedures of the Archimedes Method. *Appl. Sci.* **2019**, *9*, 583. [[CrossRef](#)]
33. Behrens, B.A.; Frischkorn, C.; Bonhage, M. Reprocessing of AW2007, AW6082 and AW7075 aluminium chips by using sintering and forging operations. *Prod. Eng.* **2014**, *8*, 443–451. [[CrossRef](#)]



© 2020 by the authors. Licensee MDPI, Basel, Switzerland. This article is an open access article distributed under the terms and conditions of the Creative Commons Attribution (CC BY) license (<http://creativecommons.org/licenses/by/4.0/>).